


Article

Effect of Trailing Edge Cylindrical Spoiler Structure on the Energy Harvesting Performance of the Oscillating Foil

Fahui Zhu ¹, Hao Li ¹, Qiang Zhang ¹, Yonghui Xie ² and Di Zhang ^{1,*} 

¹ MOE Key Laboratory of Thermo-Fluid Science and Engineering, School of Energy and Power Engineering, Xi'an Jiaotong University, Xi'an 710049, China; zhufahui@stu.xjtu.edu.cn (F.Z.); lh8023@stu.xjtu.edu.cn (H.L.); zhangqiang123@stu.xjtu.edu.cn (Q.Z.)

² State Key Laboratory for Strength and Vibration of Mechanical Structures, School of Energy and Power Engineering, Xi'an Jiaotong University, Xi'an 710049, China; yhxie@mail.xjtu.edu.cn

* Correspondence: zhang_di@mail.xjtu.edu.cn

Abstract: This study explores a novel flow control approach for enhancing the energy harvesting performance of an oscillating foil, which is a promising technology for harvesting renewable energy from wind and ocean currents. This approach involves placing a cylindrical spoiler structure at the trailing edge of the foil and investigating the effects of its diameter and spacing on the energy harvesting efficiency. The results show that the spoiler cylinders can significantly increase the energy harvesting efficiency of the foil by up to 19.26% compared to the case without them. The optimal configuration for the spoiler cylinders is found to be 11.0% of c in diameter, 0.5% of c in transverse spacing, and 0 in longitudinal spacing. Moreover, this flow control method is proven to be highly effective under a wide range of motion kinetic parameters. The findings of this study provide technical guidance for the design and implementation of oscillating foil energy harvesting devices, highlighting their practical engineering value.

Keywords: oscillating foil; energy harvesting; trailing edge; cylindrical spoiler structure



Citation: Zhu, F.; Li, H.; Zhang, Q.; Xie, Y.; Zhang, D. Effect of Trailing Edge Cylindrical Spoiler Structure on the Energy Harvesting Performance of the Oscillating Foil. *Appl. Sci.* **2024**, *14*, 561. <https://doi.org/10.3390/app14020561>

Academic Editor: Alberto Doria

Received: 5 December 2023

Revised: 22 December 2023

Accepted: 27 December 2023

Published: 9 January 2024



Copyright: © 2024 by the authors. Licensee MDPI, Basel, Switzerland. This article is an open access article distributed under the terms and conditions of the Creative Commons Attribution (CC BY) license (<https://creativecommons.org/licenses/by/4.0/>).

1. Introduction

Renewable energy represents the most promising avenue for mitigating the impact of climate change [1], serving as a viable alternative to traditional fossil fuel sources. Offshore currents, near-surface wind fields, and shallow rivers contain fluid energies that could potentially serve as renewable energy sources. However, owing to the dispersed and stochastic nature of these energies, achieving centralized and efficient harnessing poses a daunting challenge [2]. The development of effective methodologies and tools for energy harvesting has, thus far, remained elusive to researchers for an extended period of time [3]. In light of the low efficiency of conventional rotating turbines at low Reynolds numbers, McKinney [4] proposed a novel energy conversion paradigm that uses the coupling of heaving and pitching motions to harness flow energy. The oscillating foil stands out as a new energy utilization device [5] characterized by its simple structure, low oscillation speed, and low environmental demands. It is increasingly acknowledged as a technology with immense potential for development [6], gradually gaining traction in the commercial design, improvement, and adoption arena.

Enhancing the energy harvesting efficiency of oscillating foils' performance by optimizing their motion parameters has been the subject of considerable interest. Jones et al. [7] found that a sufficiently high pitching amplitude converted energy consumption into energy harvesting at a fixed frequency and amplitude. Davids [8] conducted an inquiry into the efficacy of energy harvesting via oscillating foils, with an efficiency of 30% obtained by optimizing amplitude and frequency. Tuncer and Kaya [9] enhanced aerodynamic characteristics by reducing the oscillating foils' pitching amplitude and effective angle of attack to avoid leading edge vortices, resulting in a higher thrust value.

Dumas and Kinsey [10,11] employed NACA series airfoils to study oscillating foils and presented the energy harvesting efficiency–frequency–amplitude relationship. Simpson [12] studied foils' aerodynamic characteristics in water at $Re = 13,800$ and a 90° phase angle, identifying the highest energy harvesting efficiency to be between 0.10 and 0.26 at lower frequencies for lift production. Zhu [13] explored the spoiler flow stability and energy harvesting performance relationship and revealed that peak efficiency always appears between 0.10 and 0.15 frequencies as oscillation frequency decreases. Wang reported a numerical effort in studying the performance of a sinusoidally oscillating hydrofoil at a high Reynolds number, addressing the limitation of existing research which has lower Reynolds numbers [14].

Researchers have unearthed that actively changing the shape of oscillating foils during flight, as seen in flying organisms such as birds or fish [15], can increase lift. Minor-scale deformation along the span and chord has been shown to enhance performance by Yang [16]. Le [17] proposed a rippled foil contour with ripple and curvature, concluding that slender foils exhibit a superior energy harvesting capability. Based on this premise, Le and Ko [18] discovered that spanwise bending has a smaller influence on power harvesting compared to chordwise bending. Hoke et al. [19] found that interplay between changes in shape and vortex shedding could improve energy harvesting performance, while Liu [20] determined that local deformation near the trailing edge could boost lift and improve synchronization with heaving and pitching motions. Jeanmonod [21] showed that foil deformation can enhance energy harvesting by studying the following three deformation modes: uniform deformation, leading edge deformation, and trailing edge deformation. Bai [22] analyzed the performance of the surrounding oscillating foil structure under different frequencies and local deformation amplitudes, finding that, at lower frequencies, the leading edge vortex exhibited greater connectivity with the suction side, while, at higher frequencies, there were fewer shedding vortices on the suction side. Jiang [23] proposed a C-shaped oscillating foil system and concluded that there was a stable oscillation range for pitching and heaving damping coefficients that could yield a steady energy output.

Researchers have used various methods to perturb the trailing edge flow field of oscillating foils, aiming to optimize their energy harvesting efficiency by increasing their lift. Liebeck [24] first studied the effect of Gurney flaps on the NACA airfoil and found that a 1.25% of c Gurney flap could enhance lift while reducing drag. Lee [25] optimized an underwater oscillating foil with flaps and stabilizers and found that modifying the flow through them could greatly enhance lift, while shifting the peak pressure position could reduce the moment on the flap. Xiao [26] observed a 28% efficiency increase compared to traditional blades when they explored the energy harvesting potential of vertical-axis tidal turbines using blades with fixed and oscillating flaps. Wu [27] improved efficiency by installing a smaller auxiliary oscillating foil beneath the main foil, increasing lift. Xie [28] applied an improved Gurney flap to an oscillating foil to enhance lift for energy harvesting and revealed that pitching motion consumed energy at all heights of the Gurney flap. Zhu [29] increased lift and synchronized heaving motion by using a type of adaptive Gurney flap, improving the energy harvesting capacity of the oscillating foils. Lahooti [30] found that placing a bluff body upstream significantly enhanced efficiency via two mechanisms. Sun [31] improved energy extraction from an oscillating hydrofoil by adjusting the height and motion period of a movable Gurney flap. These works provide a valuable reference for further research [32] into techniques for enhancing the efficiency of energy harvesting through oscillating foil mechanisms.

In synthesizing the existing literature, our survey reveals a multifaceted landscape in the domain of oscillating foil energy harvesting. The primary themes explored encompass the optimization of motion parameters, the alternative deformations of foil shapes, and methods for perturbing the trailing edge flow field to enhance lift and energy harvesting efficiency. However, these methods alter the original shape of the foil, such as Gurney flaps [33], trailing edge flaps [34], and spoilers [35], which may have negative effects on its structural integrity, processing complexity, applicability, and safety [36]. Notably, these

discussions form the backdrop against which our research proposal unfolds. Our focus on a tail edge cylindrical spoiler structure is motivated by the simplicity and practicality it introduces, preserving the original foil shape while innovatively enhancing vorticity generation. This unique contribution addresses gaps in the current literature by presenting a comprehensive analysis of the flow parameters, optimization methods, and applicability of this novel approach.

Based on this innovative flapping foil flow control structure, we have developed a comprehensive set of methods for analyzing the influence of flow parameters, optimization, and applicability. We have established a parametric research model featuring a cylindrical spoiler structure on the trailing edge of the foil. By comparing aerodynamic parameter profiles, pressure distributions, and flow field characteristics, we have evaluated the impact of the trailing edge cylindrical spoiler structure on energy harvesting performance. We have determined the optimal cylindrical structure parameters and selected a range of structures to vary multiple kinetic parameters, thus assessing the applicability of this flow control method across a wider range of motion parameters. Our research objectives are to design, optimize, and implement oscillating foil energy harvesting mechanisms, with the aim of making a significant contribution to the advancement of this field.

2. Numerical Modeling and Validation

2.1. Description of the Oscillating Foil Model

The paper details an inquiry into an oscillating foil model with a commonly used NACA0015 airfoil as its baseline configuration. A novel model is proposed, featuring a cylindrical spoiler structure located at the trailing edge, illustrated in Figure 1a. The parameters of the trailing edge cylindrical spoiler structure that are scrutinized in this study are expounded upon as follows: the diameter (D) of the cylinder, the transverse distance (X) from the leftmost point of the cylinder to the trailing edge of the foil, along the mid-chord direction, and the vertical distance (Y) from the center of the cylinder to the mid-chord of the foil.

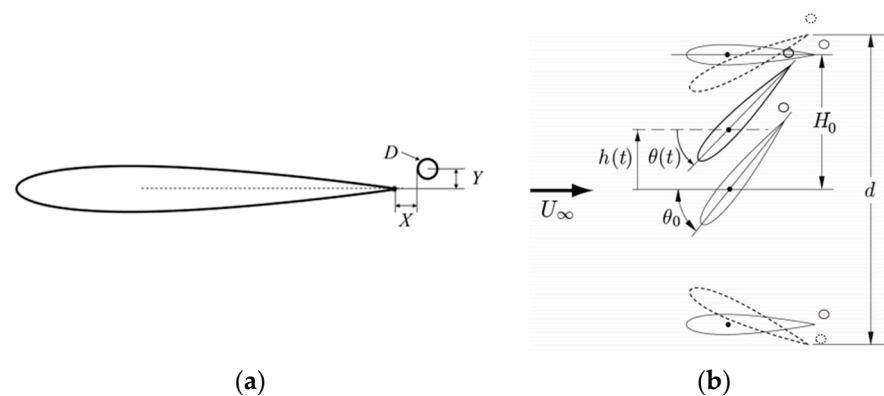


Figure 1. Schematics of the oscillating foil with a cylindrical spoiler structure at the trailing edge. (a) Oscillating foil with a cylindrical spoiler structure; (b) motion pattern of the oscillating foil.

Presently, studies concerning energy harvesting from oscillating foils predominantly employ an actively coupled motion mode that involves both pitching and heaving. This motion pattern involves a rotational pitching motion around the axis of rotation, accompanied by a vertical heaving oscillation, as depicted in Figure 1b. These two motions are self-contained and are characterized by the classic sinusoidal waveform expressed as follows:

$$\theta(t) = \theta_0 \sin(2\pi ft) \quad (1)$$

$$h(t) = H_0 \sin(2\pi ft + \phi) \quad (2)$$

where $\theta(t)$ is the instantaneous pitching amplitude/rad; $h(t)$ is the instantaneous heaving position/m; θ_0 is the pitching amplitude/rad; H_0 is the heaving amplitude/m; f is the

oscillating frequency/Hz; t is the motion time/s; and ϕ is the phase difference between the coupled heaving and pitching motions, which is fixed at 90° in the study of this paper.

The non-dimensional frequency, denoted as f^* , is defined as follows:

$$f^* = \frac{fc}{U_\infty} \quad (3)$$

where c denotes the chord length of the foil/m, and U_∞ represents the freestream velocity far upstream of the oscillating foil.

The power extracted from the flow field can be decomposed into the following two components: one from the heaving process and the other one from the pitching process. The expressions of the instantaneous total power are as follows:

$$P(t) = F_y(t) \cdot V_y(t) + M(t) \cdot \omega(t) \quad (4)$$

where $P(t)$ is the instantaneous total power/W; $F_y(t)$ is the instantaneous aerodynamic lift in the y-direction/N; $V_y(t)$ is the instantaneous velocity of the foil during the heaving motion/ $\text{m} \cdot \text{s}^{-1}$; $M(t)$ is the instantaneous torque of the foil's pitching center/ $\text{N} \cdot \text{m}^{-1}$; and $\omega(t)$ is the instantaneous rotational angular velocity of the pitching motion/ $\text{rad} \cdot \text{s}^{-1}$.

The corresponding instantaneous total power coefficient $C_P(t)$ and the average total power coefficient C_{Pm} of the oscillating foil during one cycle are the following:

$$C_P(t) = \frac{P(t)}{\frac{1}{2}\rho U_\infty^3 cL} \quad (5)$$

$$C_{Pm} = \frac{1}{T} \int_0^T \frac{P(t)}{\frac{1}{2}\rho U_\infty^3 cL} dt \quad (6)$$

where T is the motion period of oscillation/s; ρ is the density of the incoming fluid/ $\text{kg} \cdot \text{m}^{-3}$; and L is the spreading length of the foil/m. In this paper, the latter is considered to be a unit length for the two-dimensional flow investigation discussed.

The instantaneous lift coefficient $C_{Fy}(t)$ and torque coefficient $C_M(t)$ of the oscillating foil are as follows:

$$C_{Fy}(t) = \frac{F_y(t)}{\frac{1}{2}\rho U_\infty^2 cL} \quad (7)$$

$$C_M(t) = \frac{M(t)}{\frac{1}{2}\rho U_\infty^2 c^2 L} \quad (8)$$

The corresponding instantaneous heaving power coefficients $C_{Py}(t)$ and instantaneous pitching power coefficients $C_{P\theta}(t)$ are the following:

$$C_{Py}(t) = \frac{F_y(t) \cdot V_y(t)}{\frac{1}{2}\rho U_\infty^3 cL} \quad (9)$$

$$C_{P\theta}(t) = \frac{M(t) \cdot \Omega(t)}{\frac{1}{2}\rho U_\infty^3 cL} \quad (10)$$

The energy harvesting efficiency η is given by the following equation:

$$\eta = C_{Pm} \frac{c}{d} \quad (11)$$

where d refers to the distance covered by the oscillating foil in the direction of the heaving motion during one cycle/m, as illustrated in Figure 1b.

2.2. Numerical Methodology

This paper employs the finite volume method and the well-established CFD solver Fluent to solve the two-dimensional, transient, and incompressible Navier–Stokes equations for the oscillating foil problem. The pressure-based coupled (SIMPLE) segregated algorithm is used to evaluate the pressure gradient in the momentum equation. For the stability and convergence, the convection terms and the diffusion term are discretized by a second-order accurate upwind scheme and a second-order central-differencing scheme, respectively.

To simulate the coupled heaving and pitching motion of the oscillating foil with a large amplitude, the sliding mesh technique is applied by dividing the fluid domain into two sub-domains, as shown in Figure 2. The inner domain undergoes a rigid body motion, which means that the motion of the oscillating foil is prescribed and fixed during the simulation. The outer domain, on the other hand, needs to re-mesh to adapt to the oscillating foil's large-amplitude. The mesh slides and deforms according to the motion of the foil, enabling an accurate simulation of fluid–structure coupling interactions. A user-defined function (UDF) is used to customize the motion trajectory.

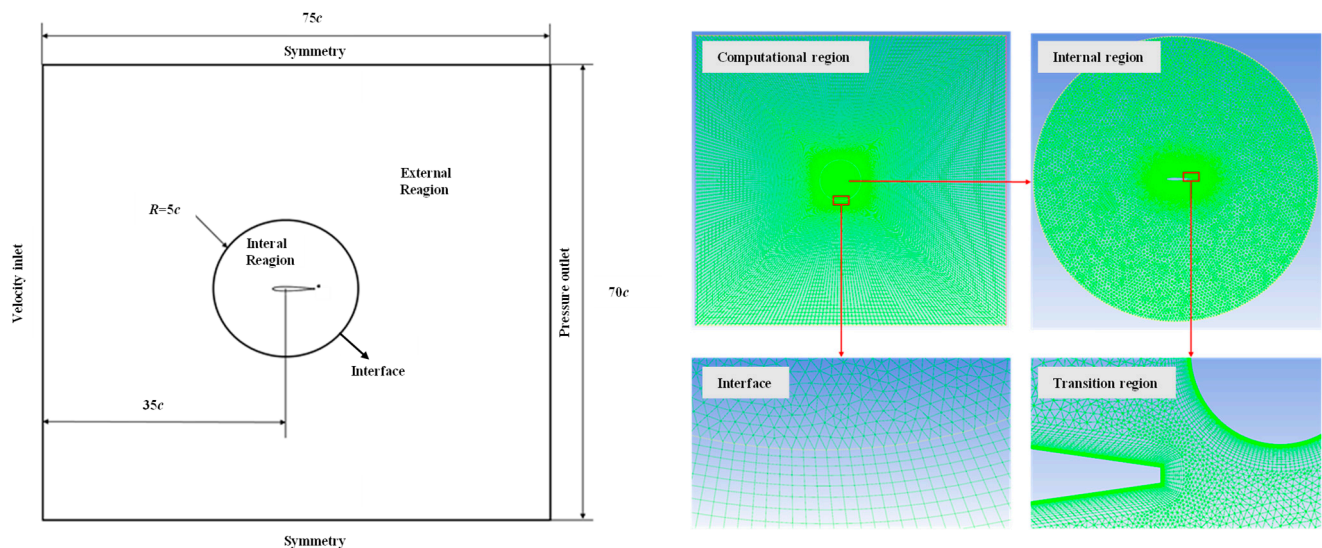


Figure 2. Mesh details with boundary conditions.

We start with the baseline configuration NACA0015 airfoil under the condition of $Re = 1100$, $H_0/c = 1$, $f^* = 0.14$, $\theta_0 = 76.3^\circ$, and $\phi = 90^\circ$, which is selected based on Kinsey [11]. Since there are no major qualitative changes in the cycles of power extraction except for slightly amplified extrema associated with amplified force coefficients, this paper does not study a higher Re .

The inlet velocity is calculated from $Re = 1100$ using the URANS approach based on the Spalart–Allmaras model. The boundary interface serves to link the inner and outer domains within the simulation. Symmetric no-slip boundary conditions are imposed on the upper and lower boundaries to ensure no flow through these boundaries. The entrance and exit boundary conditions are applied to the left and right boundaries, respectively, to simulate the flow entering and exiting the domain. The oscillating foil and cylinder are located in the inner domain, with the cylinder placed at the trailing edge. The outer domain measures $75c \times 70c$ with the pitching axis of the oscillating foil located $35c$ from the inlet boundary. A circular interface with a radius of $5c$ connects the inner and outer domains. The outer domain is partitioned into a structured quadrilateral mesh using O-type partitioning to enhance mesh quality. As shown in Figure 2, the red box shows the grid area that needs further display, and along the direction of the red arrow, a partial enlargement of the grid drawing details is given. The inner domain is partitioned into a triangular mesh with boundary layers applied to the oscillating foil and cylinder surfaces. The initial layer mesh thickness of the boundary layer is set to $10^{-5}c$, ensuring that the y^+

value remains below 1 throughout the simulation. To reduce numerical calculation errors and flow field fluctuations caused by large variations in mesh size, denser mesh nodes are placed on the foil and cylinder surfaces due to the relatively small size of the trailing edge cylinder and its proximity to the foil.

2.3. Validation of Computation

During the oscillation of the flapping foil, continuous changes occur in both its position and velocity, accompanied by a significant non-steadiness in the surrounding flow field. Given these dynamic circumstances, the grid division of the flow field and time step utilized in numerical simulation iterations can significantly impact calculation outcomes. To ensure the independence of numerical solutions from the chosen time step and grid, it is imperative to conduct verification tests for time step independence and grid independence before delving into specific research endeavors.

To investigate time step independence, three distinct time intervals (quantified as 1200, 2400, and 4800 steps per cycle), have been thoroughly examined. In Figure 3, the change values of the resistance coefficient (C_D), lift coefficient (C_L), and power coefficient (C_P) throughout one cycle are depicted for different time steps. The curves converge notably at 2400 and 4800 steps per cycle, demonstrating excellent agreement. For clarity, Table 1 presents the average power coefficient values and deviations for different time steps. Notably, in reference to the third time step, the relative difference between intermediate time step 2 and time step 3 is merely 0.25%. Striking a balance between calculation accuracy and computational cost, we have selected 2400 steps per cycle for subsequent calculations.

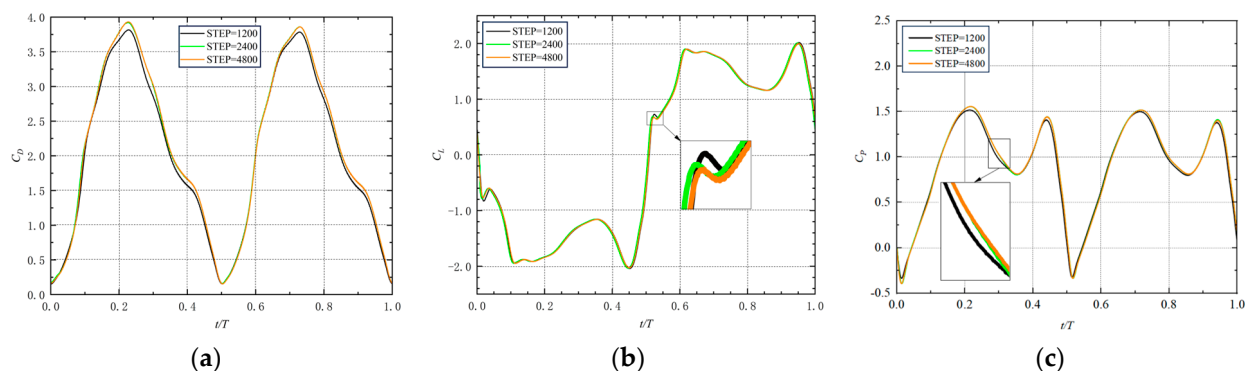


Figure 3. Time independence verification curve. (a) Resistance coefficient curve; (b) lift coefficient curve; and (c) power coefficient diagram.

Table 1. Average total power coefficients and deviations at different time steps.

Time Criterion	Time Steps/Cycle	Cells	C_{Pm}	Deviation
Coarse	1200	1.5×10^5	0.8954	1.87%
Medium	2400	1.5×10^5	0.9102	0.25%
Fine	4800	1.5×10^5	0.9125	-

The mesh independence of the NACA0015 airfoil is further verified under conditions analogous to a time independence verification, i.e., using three mesh strategies with airfoil surface sizes set to 0.002 m, 0.001 m, and 0.0005 m, resulting in grid quantities of 7.0×10^4 , 1.5×10^5 , and 3.2×10^5 . In Figure 4, the change values of resistance coefficient C_D , lift coefficient C_L , and power coefficient C_P in one cycle under three grid numbers are presented. Notably, for the medium and fine meshes, the curves of the coefficients tend to be consistent. The average power coefficient values and deviations under different grid numbers are provided in Table 2, with a relative difference between the medium and fine meshes of 0.16%. Thus, grid number 1.5×10^5 is adopted for subsequent calculations.

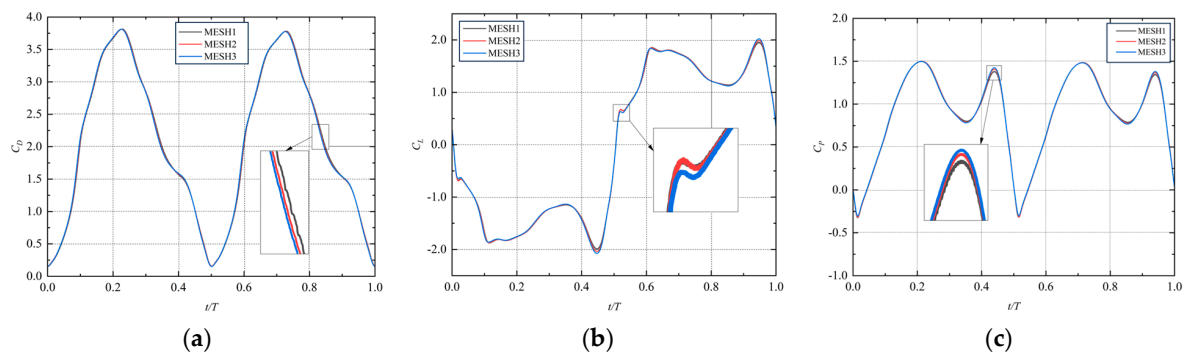


Figure 4. Grid number independence verification curve. (a) Resistance coefficient curve; (b) lift coefficient curve; (c) power coefficient diagram.

Table 2. Average total power coefficient and deviation for different numbers of mesh cells.

Mesh Criterion	Surface Grid Size/m	Cells	Time Steps/Cycle	C_{Pm}	Deviation
Coarse	0.002	7.0×10^4	2400	0.8916	0.47%
Medium	0.001	1.5×10^5	2400	0.8944	0.16%
Fine	0.0005	3.2×10^5	2400	0.8958	-

To validate the established numerical simulation method, calculations with time steps of 2400 and a grid number of 1.5×10^5 are compared with Kinsey [11]. Figure 5a–c display the comparison results under the chosen operating condition, demonstrating a remarkable congruence in the dynamic transient characteristic parameters. Additionally, a further validation against Kinsey’s extended research [37] is presented in Figure 5d, where the energy harvesting efficiency of the flapping foil exhibits a consistent congruence, particularly at higher levels of energy harvesting efficiency.

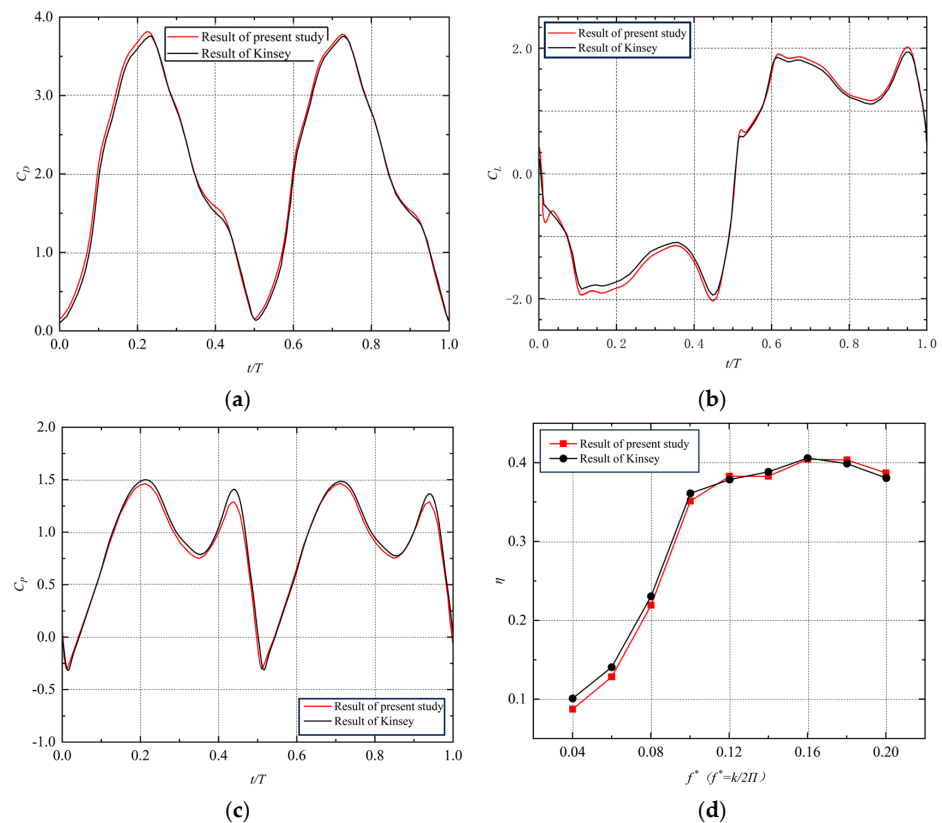


Figure 5. Comparison between the results of the present study with Kinsey’s results. (a) Resistance coefficient curve; (b) lift coefficient curve; (c) power coefficient diagram; (d) efficiency curve varying f^* .

In summary, the judicious selection of appropriate time increments and grid configurations has substantiated the elevated precision and reliability of our numerical simulation approach.

3. Results and Discussions

Aiming to enhance the energy harvesting efficiency of oscillating foils, this investigation introduces an innovative flow control methodology for analyzing the impact of flow parameters and their optimization and conducting an applicability assessment. Utilizing a NACA0015 foil model with a cylindrical spoiler structure at the trailing edge, we examine the effects of the spoiler structure (cylinder diameter, transverse spacing, and longitudinal spacing) on the energy harvesting performance. Optimal cylindrical structure parameters are identified, and a set of structures is chosen to evaluate the applicability of this flow control approach across a broader range of motion parameters.

3.1. Effect of Cylinder Diameter on the Energy Harvesting Performance

Under specific conditions ($\theta_0 = 50^\circ$, $\phi = 90^\circ$, $H_0/c = 1$, $f^* = 0.14$, and $Re = 1100$), the diameter (D) of the trailing edge cylinder is varied, ranging from 1.0% to 11.0% of the chord length, while maintaining constant transverse spacing ($X = 0.5\%$ of c) and longitudinal spacing ($Y = 0$). The aerodynamic performance of the oscillating foil is assessed under identical conditions to analyze variations with and without cylinders of different diameters.

In Figure 6a, the curves depicting the mean power coefficient and efficiency of the oscillating foil across various cylindrical diameters are presented. The dashed lines represent the original foil without a cylinder, with mean power coefficient and efficiency values of 0.4042 and 17.60%, respectively. A noticeable enhancement in energy harvesting performance is observed with an increasing cylinder diameter. Specifically, at a cylinder diameter of 11.0% of c , the average total power coefficient reaches 0.4820, indicating a substantial 19.26% improvement compared to energy harvesting without a cylinder.

An in-depth investigation into the instantaneous total power coefficient reveals fluctuation patterns for distinct cylinder diameters, as shown in Figure 6b. Notably, the trend exhibits a diminishing steepness beyond a cylinder diameter of 7.0% of c , which is not depicted beyond this limit. The distinctions between curves for various cylindrical diameters are primarily evident in the range around peak and valley values. Overall, the energy capturing efficiencies of the oscillating foil with a cylinder surpass those of the foil without. There exists a direct correlation between the diameter of the trailing edge cylinder and the peak value, suggesting that a larger cylinder diameter leads to a higher peak value. This trend aligns with observations in the mean power coefficient, emphasizing the comparable nature of trends in mean power coefficient and energy capturing efficiency.

Figure 6c,d depict the variation of the instantaneous lift coefficient and the instantaneous heaving power coefficient of the oscillating foil, respectively. As the cylinder diameter increases, the peak values of the instantaneous lift coefficient and heaving power coefficient of the foil increase, while the valley values decrease. The maximum instantaneous heaving power coefficient occurs during the interval between the time of the instantaneous lift coefficient and the heaving speed reaching its maximum. Despite a synchronous difference existing between lift and heaving speed, the foil predominantly performs positive work in the direction of heaving throughout most of the cycle.

Figure 6e,f show the curves of the instantaneous torque coefficient and the instantaneous pitching power coefficient of the oscillating foil, respectively. The foil with a cylindrical spoiler structure has larger maximum values and smaller valley values for both coefficients than the foil without the spoiler structure. The instantaneous torque coefficients reach their maxima around $t/T = 0.2$ and 0.7 , while the instantaneous pitching angular velocity has its minimum value at $t/T = 0.5$. The cylinder diameter does not change the timing of the maxima. The instantaneous pitching power coefficient, which is directly proportional to the product of the instantaneous torque coefficient and the pitching angular velocity, has its second peak between 0.4 and 0.5 cycles. In this interval, both the instantaneous torque coefficient and the pitching angular velocity are negative. However, the

direction of the instantaneous torque does not match well with the direction of the pitching angular velocity over the entire cycle. The time difference between them is almost half of the cycle, which makes the instantaneous pitching power coefficient positive for most of the first half-cycle and negative for most of the second half-cycle. As a result, the mean pitching power coefficient over the entire cycle is relatively low, and it has little contribution to the overall average total power coefficient. This indicates that the foil mainly harvests energy through heaving motions.

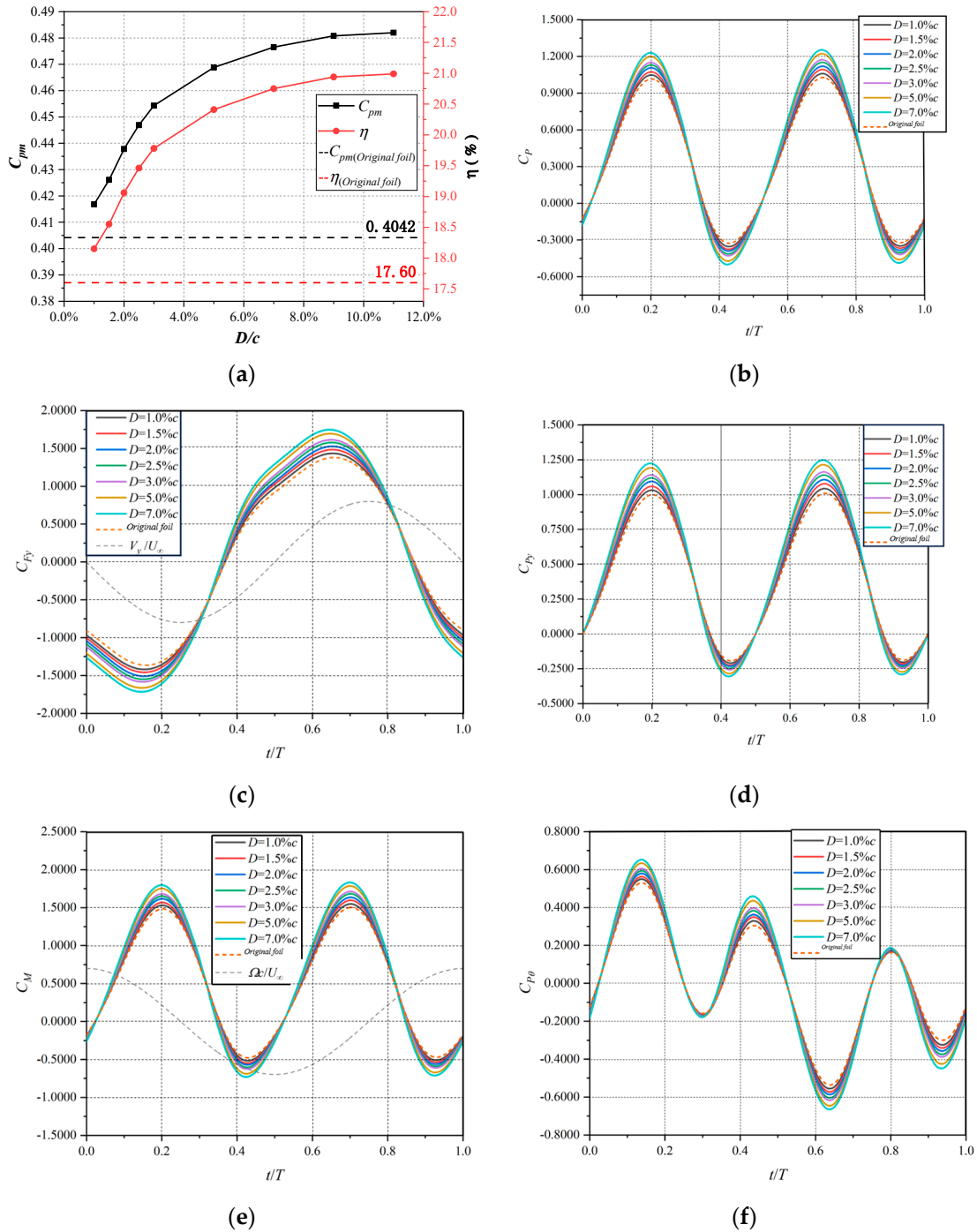


Figure 6. Comparison of C_{Pm} & η , C_p , C_{Fy} , C_{py} , C_M , and $C_{p\theta}$ of the oscillating foil with/without cylindrical spoiler structure at the trailing edge for different diameters: (a) Average total power coefficient and efficiency; (b) instantaneous total power coefficient; (c) instantaneous lift coefficient; (d) instantaneous heaving power coefficients; (e) instantaneous torque coefficient; and (f) instantaneous pitching power coefficients.

To comprehensively understand the aerodynamic flow field of oscillating foils and assess the influence of a cylindrical spoiler structure at the trailing edge on their energy harvesting performance, we employ pressure distribution and streamlines near the trailing edge for a further analysis, as illustrated in Figure 7. Specifically, we focus on two critical moments ($t/T = 0.25$ and 0.75) during the entire motion cycle, representing opposite states in terms of pitching direction, heaving direction, and angle of attack.

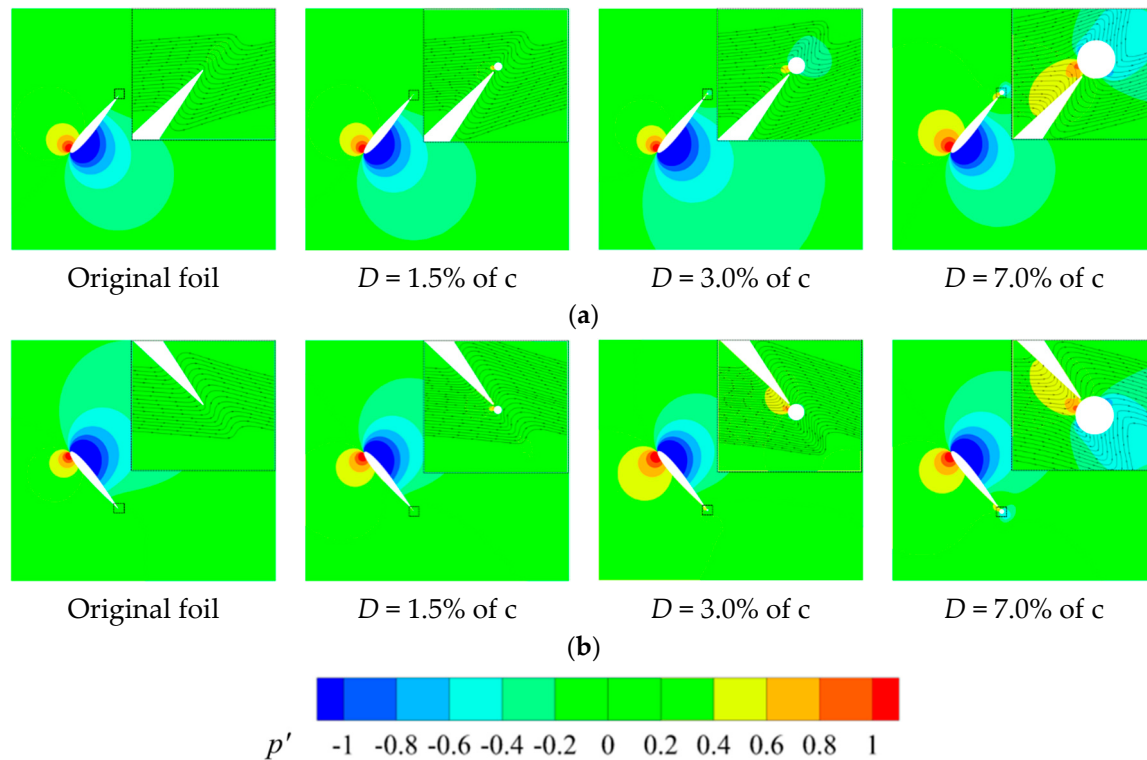


Figure 7. Pressure coefficient cloud and streamline of the oscillating foil with/without cylindrical spoiler structure at the trailing edge for different diameters. (a) $t/T = 0.25$; (b) $t/T = 0.75$.

In the absence of a cylinder, the fluid flow near the trailing edge appears smooth. Taking $t/T = 0.2$ as an example, as the fluid traverses the foil's surface, an obstruction materializes on the upper surface, causing a reduction in fluid velocity and an increase in pressure. Consequently, a heightened pressure zone manifests on the upper surface at the forefront of the foil, while a low-pressure region emerges on the lower surface.

With the introduction of the cylinder, a high-pressure zone forms on the cylinder surface. As depicted in the diagram, the increase in cylinder diameter not only amplifies the high-pressure zone but also extends its influence across a broader range of the flow field. This expansion is visually represented in the diagram, highlighting the larger area of high-pressure zone formation. Moreover, the initial parameter fixing the longitudinal spacing to 0, coupled with the symmetry of the cylinder about the median chord of the foil, leads to notable effects. Specifically, the presence of the cylinder enhances fluid backflow and accentuates pressure differentials near the trailing edge. The influence of the cylinder becomes more pronounced with an increasing diameter, intensifying the fluid reflow effect. This augmentation results in a heightened total pressure differential on the foil. Consequently, this intensified pressure distribution contributes to an elevation in the lift of the foil. Simultaneously, there is a corresponding increase in the instantaneous heaving power coefficient. These combined effects synergistically contribute to enhancing the overall energy harvesting efficiency of the system.

Figure 8 shows the pressure coefficient distribution on the foil's surface for different cylinder diameters at t/T s of 0.25 and 0.75, which are two critical moments in the motion

cycle. The upper and lower curves correspond to the upper and lower surfaces of the foil, respectively, but they switch roles at a t/T of 0.75. The analysis of pressure coefficient distribution provides crucial insights into how the cylindrical spoiler structure influences the pressure dynamics on the foil's surface, further elucidating the mechanisms contributing to enhanced lift and energy harvesting efficiency.

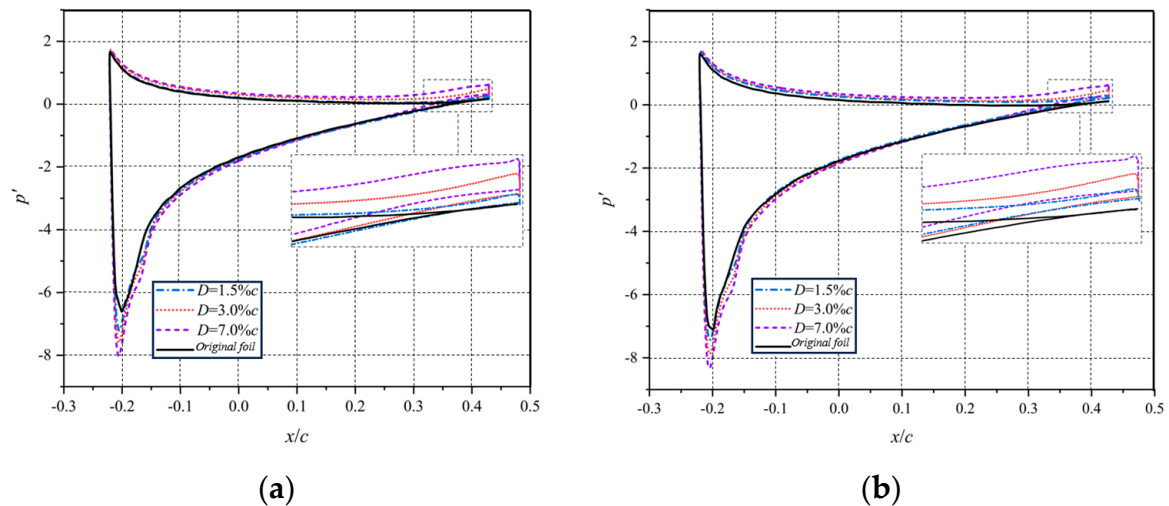


Figure 8. Distribution of the pressure coefficient on the surface of the oscillating foil with/without a cylindrical spoiler structure at the trailing edge for different diameters. (a) $t/T = 0.25$; (b) $t/T = 0.75$.

The flow characteristics and the cylinder effect are almost the same for both moments. For the original foil without the cylindrical spoiler structure, the pressure coefficient curves almost completely overlap at the trailing edge, signifying a negligible pressure disparity between the upper and lower surfaces. The resulting additional force on the trailing edge is minimal, roughly around the zero point. Nonetheless, in the event that the trailing edge incorporates a cylinder, the pressure coefficient curves pertaining to the upper and lower surfaces shift in an upward direction, while also assuming a more distinct form. Moreover, the pressure coefficient curves that exist between these two surfaces exhibit increasingly greater spacing as the diameter of the cylinder grows larger. This indicates that the difference between the upper surface pressure and the lower surface pressure is increasing, leading to a greater extra force on the trailing edge of the foil. This finding confirms the foil's increased lift and energy collection efficiency, in accordance with the law of energy conservation.

3.2. Effect of Cylinder Transverse Spacing on the Energy Harvesting Performance

Retaining the same cylindrical diameter ($D = 3.0\%$ of c) and longitudinal spacing ($Y = 0$), the cylindrical transverse spacing X is varied at discrete intervals, from 0.5% of c to 65.5% of c . Subsequently, we evaluate the foils' aerodynamic traits under identical conditions to investigate the impact of cylinders with varying transverse spacing X on the efficacy of energy extraction.

Figure 9a illustrates the mean total power coefficient during one cycle and the efficiency of the oscillating foil with varying X of the cylinders. The transverse spacing ranging from 0.5% of c to 2.5% of c yields a higher energy harvesting efficiency than the foil without cylinders. At $X = 0.5\%$ of c , the average total power coefficient is 0.4543 , with an energy harvesting efficiency of 19.78% , showing a 12.39% improvement compared to the configuration without cylinders. Conversely, the transverse spacing in the range of 3.5% of c to 65.5% of c results in a lower energy harvesting efficiency. When $X = 9.5\%$ of c , the energy harvesting efficiency is 2.10% lower than that of the original foil without cylinders, representing the minimum efficiency in the evaluated operating range. Beyond $X = 9.5\%$ of c , the efficacy of energy harvesting decreases, becoming equivalent to the foil

without a cylindrical spoiler structure at $X = 65.5\%$ of c . Practical applications should avoid unfavorable transverse spacing to enhance energy harvesting efficiency.

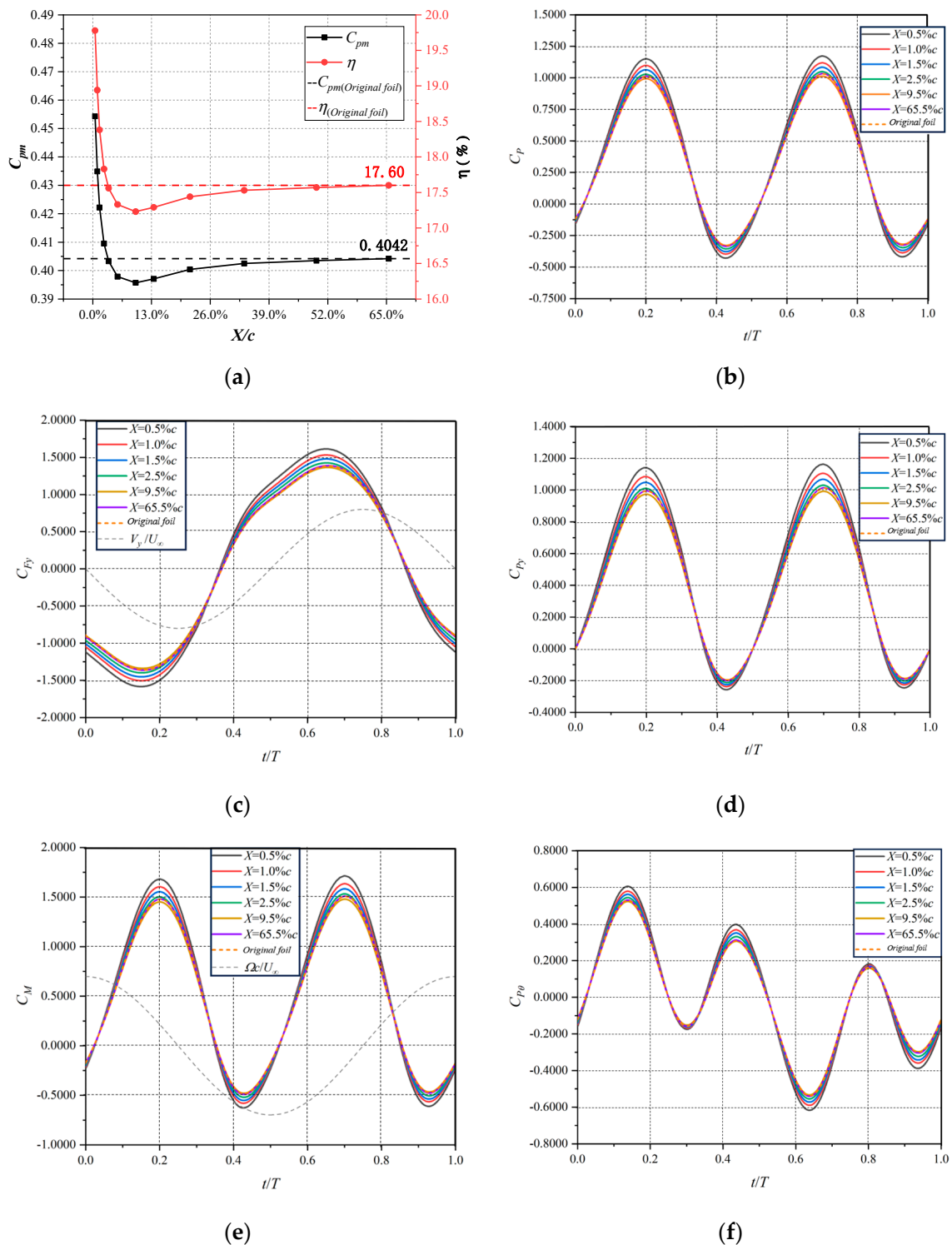


Figure 9. Comparison of C_{pm} & η , C_p , C_{Fy} , C_{Py} , C_M , and $C_{P\theta}$ of the oscillating foil with/without a cylindrical spoiler structure at the trailing edge for different cylinder transverse spacings: (a) Average total power coefficient and efficiency; (b) instantaneous total power coefficient; (c) instantaneous lift coefficient; (d) instantaneous heaving power coefficients; (e) instantaneous torque coefficient; and (f) instantaneous pitching power coefficients.

Figure 9b presents curves depicting the fluctuation of the instantaneous total power coefficient for the oscillating foil with different cylindrical transverse spacings. For X equal to or less than 9.5% of c , the instantaneous total power coefficient near both the peak and the valley decreases as X increases, with smaller transverse spacing exhibiting the best energy harvesting performance. When the spacing is greater than 9.5% of c , the instantaneous total power coefficient near the peak slightly increases, and the change near the valley is not obvious, resulting in a slight improvement in energy harvesting performance until $X = 65.5\%$ of c .

Figure 9c,d show the variations in instantaneous lift coefficients and heaving power coefficients. For transverse spacing less than or equal to 9.5% of c , the instantaneous lift coefficient decreases near the peak and increases near the valley as the transverse spacing increases. Simultaneously, the instantaneous heaving power coefficient declines near the peak and rises near the valley.

Figure 9e,f illustrate the variation of the instantaneous torque coefficient and the instantaneous pitching power coefficient. The maximum instantaneous torque coefficient occurs around $t/T = 0.2$ and 0.7 , while the instantaneous pitching angular velocity achieves its minimum value at $t/T = 0.5$. The transient pitching power coefficient exhibits asymmetry between the front and rear half-cycles in one cycle, resulting in a small average pitching power coefficient, contributing little to the overall average total power coefficient.

The presence of the cylinder introduces disruptions to the fluid flow, generating a heightened pressure region on the cylinder's surface, as depicted in Figure 10. The dynamic interaction between the oscillating foil and the cylinder induces variations in pressure distribution and flow field.

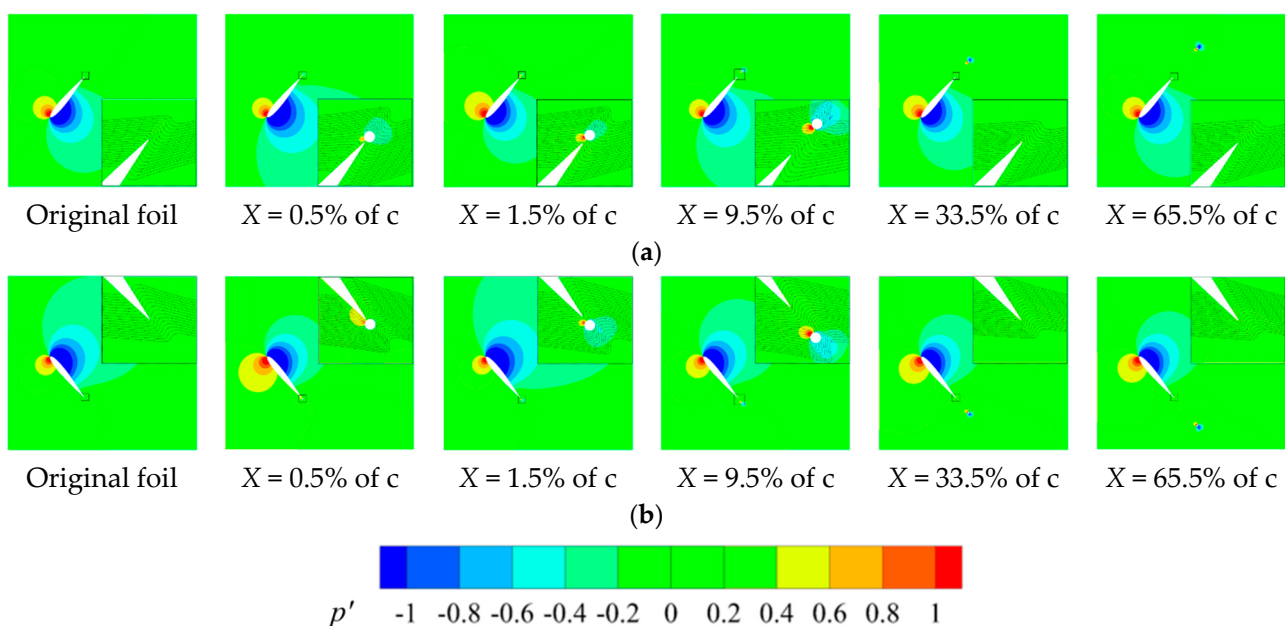


Figure 10. Pressure coefficient cloud and streamline of the oscillating foil with/without a cylindrical spoiler structure at the trailing edge for different cylinder transverse spacings. (a) $t/T = 0.25$; (b) $t/T = 0.75$.

To delve further into the detailed dynamics, when the oscillating foil executes a downward motion, a distinctive elevated pressure region emerges on the upper side of the cylinder's leading edge. Conversely, during the upward motion, the high-pressure region shifts in the opposite direction. For instance, in the case of the oscillating foil with a cylindrical spoiler structure at X of 0.5% of c and 1.5% of c during $t/T = 0.25$, the trailing edge coincides with the elevated high-pressure region at the front of the cylinder. This alignment induces a disturbance that significantly disrupts the pressure equilibrium at the trailing edge point of the cylinder, presenting a departure from the scenario in the

absence of a cylinder. The consequence is a localized increase in the pressure coefficient. This localized pressure variation is most pronounced in the pressure coefficient distribution observed at X of 1.5% of c .

As the distance between the cylinder and the trailing edge increases, the impact of localized pressure alterations and their influence on the intricate flow field diminishes. This diminishing influence becomes notably marginal at a transverse distance of 65.5% of the chord length. Consequently, the pressure and streamline distribution approach that of the original foil. Therefore, at a transverse distance of 65.5% of c , the energy harvesting performance becomes comparable to that of the original foil.

The distribution of the pressure coefficient on the surface of the oscillating foil, with f corresponding to a different X , is displayed in Figure 11. This depiction illuminates the evolving pressure dynamics and their impact on lift force and energy harvesting performance. When $X = 0.5\%$ of c , the envelope of the pressure coefficient distribution is at its maximum, resulting in the largest pressure difference and lift force, hence displaying optimal energy harvesting performance. As $X = 1.5\%$ of c , the difference between the upper surface and the lower surface decreases, compared to 0.5% of c , indicating a reduction in energy harvesting performance. At 9.5% of c , the direction of the pressure difference on the trailing edge indicates is opposite of the leading edge's opposing direction, and the energy harvesting performance is further weakened, being the lowest among the compared conditions. Finally, when X is 65.5% of c , the pressure coefficient distribution curves of the upper and the lower surfaces nearly overlap, resulting in the pressure being almost equal on both sides, and the influence of the trailing edge cylinder reduced to the minimum, displaying similar energy harvesting characteristics as those of the original foil without the trailing edge cylinder.

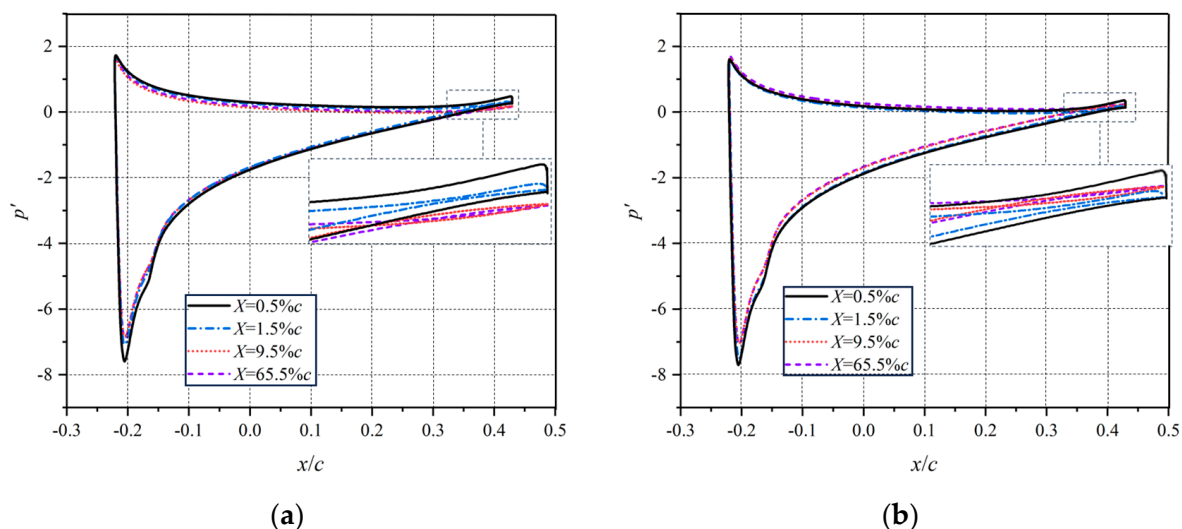


Figure 11. Distribution of the pressure coefficient on the surface of the oscillating foil with/without a cylindrical spoiler structure at the trailing edge for different cylinder transverse spacings. (a) $t/T = 0.25$; (b) $t/T = 0.75$.

3.3. Effect of Cylinder Longitudinal Spacing on the Energy Harvesting Performance

Maintaining the trailing edge cylinder diameter ($D = 3.0\%$ of c) and transverse spacing ($X = 0.5\%$ of c) constant whilst varying the longitudinal spacings (Y) at 0%, 0.5%, 1.0%, 2.0%, 4.0%, and 6.0% of the chord's length provides valuable insights into the influence of these parameters on the energy harvesting performance.

As illustrated in Figure 12a, an increase in Y results in a diminishing rate of decrease in the mean total power coefficient and efficiency of the oscillating foil. Even with $Y = 6.0\%$ of c , the trailing edge cylinders slightly enhance the energy harvesting performance, emphasizing their persistent positive impact.

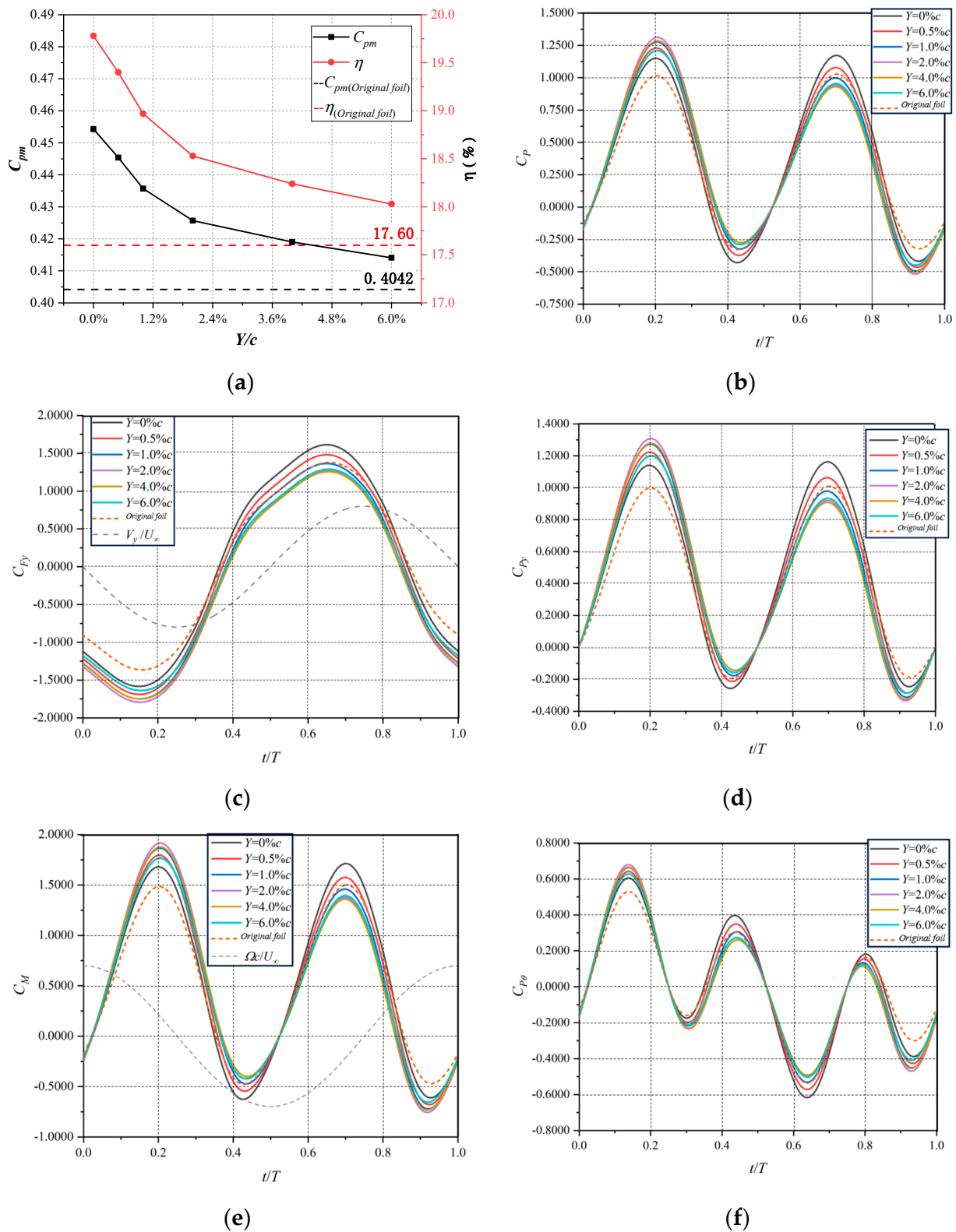


Figure 12. Comparison of C_{Pm} & η , C_p , C_{Fy} , C_{Py} , C_M , and $C_{P\theta}$ of the oscillating foil with/without a cylindrical spoiler structure at the trailing edge for different cylinder longitudinal spacings: (a) Average total power coefficient and efficiency; (b) instantaneous total power coefficient; (c) instantaneous lift coefficient; (d) instantaneous heaving power coefficients; (e) instantaneous torque coefficient; and (f) instantaneous pitching power coefficients.

Figure 12b illustrates the instantaneous total power coefficient of the oscillating foil for various longitudinal spacings. In the absence of cylinders or with zero longitudinal spacing, the curves exhibit consistent shapes in both half-cycles. However, the introduction of cylinders along the foil's central axis with nonzero longitudinal spacing disrupts this symmetry within each cycle, particularly affecting the peak and trough values. The most significant deviation occurs at 2% of c , enhancing the performance in the first half-cycle but significantly reducing it in the second half-cycle. Notably, only at zero longitudinal spacing do both half-cycles display improved performance, resulting in the best overall outcome. Generally, for an oscillating foil with a cylinder at the trailing edge, the enhancement in the energy harvesting performance during the first half-cycle outweighs the decline in the second half-cycle, resulting in a higher combined performance compared to a configuration without a cylinder. However, this improvement diminishes with increasing longitudinal spacing.

Figure 12c,d present the instantaneous lift coefficient and the instantaneous heaving power coefficient separately. In the first half-cycle, the trough values of the lift coefficient are lower than those without cylinders, while only the peak values at $Y = 0\%$ of c and 0.5% of c surpass those without cylinders in the second half-cycle. The synergy between instantaneous lift and heaving velocity near their peak and trough values is reflected in the relationship with the instantaneous heaving power coefficients. The presence of the cylinder at the trailing edge enhances the average total power coefficient in the first half-cycle, significantly boosting the energy harvesting performance. However, in the second half-cycle, only zero longitudinal spacing improves performance, while most other spacings lead to its reduction. Consequently, as longitudinal spacing increases, the overall performance improvement weakens gradually.

For each operating condition, two peaks and two troughs appear in the torque coefficient curves, while three peaks and three troughs are evident in the pitching power coefficient curves, as shown in Figure 12e,f. The primary differences between the curves occur around the peaks and troughs. The torque coefficients with a cylindrical foil are larger than those without at a t/T of 0.2 but are only the same for $Y = 0\%$ of c and 0.5% of c at a t/T of 0.7. The opposite patterns emerge at t/T_s of 0.4 and 0.9. Since the instantaneous pitching angular velocity is maximal at t/T_s of 0 and 1 and minimal at a t/T of 0.5, it influences the timing of the peak and trough values in both coefficients, resulting in multiple peaks and troughs in the pitching power coefficient curve. The first peak of this curve slightly precedes that of the moment coefficient curve, reflecting the impact of adding cylinders or changing their longitudinal spacing in both coefficients. The second peak of the pitching power coefficient curve occurs between t/T_s of 0.4 and 0.5, aligning with the first trough of the moment coefficient curve. The second trough of the pitching power coefficient curve precedes a t/T of 0.7, displaying an opposite pattern to the second peak of the torque coefficient curve due to the reversal of the pitching angular velocity at this point. The third trough of the pitching power coefficient curve mirrors the second trough of the torque coefficient curve. In summary, there is a lack of synchronization between the direction of the transient torque and the direction of the foil pitching motion during one cycle; that is, they differ for almost half of each cycle, resulting in a near-zero average transient pitching power coefficient for the foil over each cycle, weakly affecting its total energy harvesting performance.

Figure 13 presents a comprehensive analysis of the pressure coefficient distribution and streamlines, offering detailed insights into the intricate fluid dynamics around the oscillating foil with varying longitudinal spacings of the cylinder. At $Y = 0\%$ of c , the presence of the cylinder enhances fluid backflow on both surfaces of the foil's trailing edge, leading to increased pressure coefficients on both surfaces near the trailing edge. This augmentation results in increased pressure coefficients on both the upper and lower surfaces near the trailing edge. The localized pressure increase plays a pivotal role in generating a lifting effect on the trailing edge during both downward and upward heaving

motions. This lifting effect contributes to an overall augmentation of the lift coefficient and energy harvesting performance in the oscillating foil.

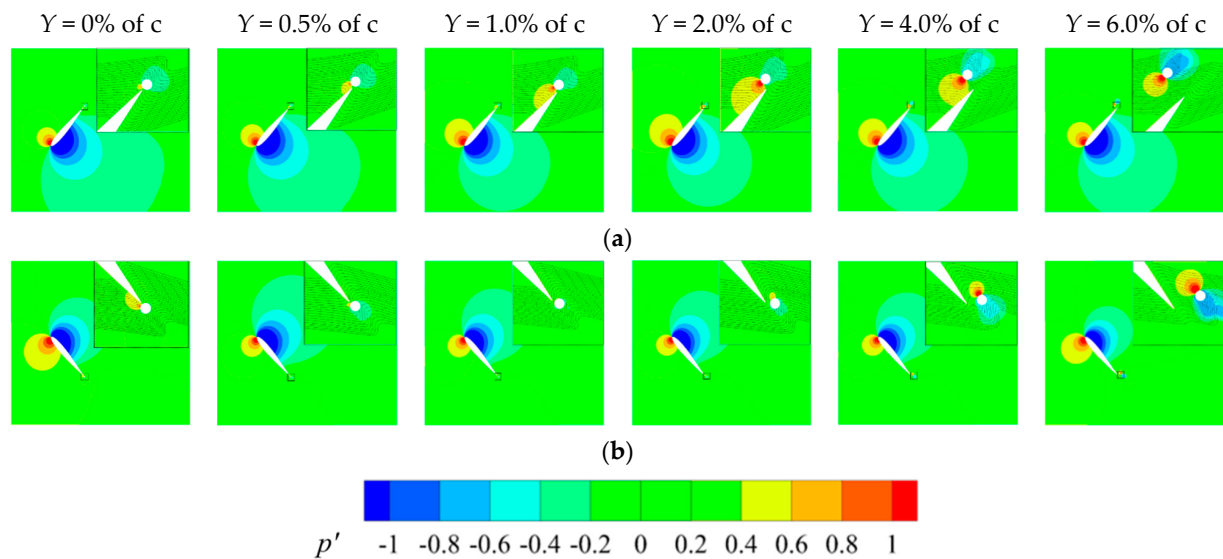


Figure 13. Pressure coefficient cloud and streamline of the oscillating foil with/without a cylindrical spoiler structure at the trailing edge for different cylinder longitudinal spacings. (a) $t/T = 0.25$; (b) $t/T = 0.75$.

As the longitudinal spacing of the cylinder increases, more nuanced examination reveals how the localized high-pressure area at the forefront of the cylinder interacts differently during downward and upward heaving due to deviation from the foil mid-chord. This discrepancy becomes notably evident in the pressure coefficient distribution when $t/T = 0.75$. Specifically, at $Y = 0.5\%$ of c , the high-pressure area at the forefront of the cylinder positively influences the trailing edge of the flutter. However, a significant shift occurs when the longitudinal spacing of the cylinder exceeds or equals 2.0% of c . The altered flow conditions result in the cylinder exhibiting completely opposite effects during the initial and latter half-cycles of the foil. This observed trend indicates a gradual weakening of the enhancement effect on the energy harvesting performance and further underscores the intricate interplay between flow dynamics, vortices, and energy harvesting efficiency.

The distribution curves of the surface pressure coefficient of the foil for different longitudinal spacings of the cylinder are presented in Figure 14. At $Y = 0\%$ of c , the corresponding curve exhibits the smallest range of the pressure coefficient distribution envelope, resulting in the foil experiencing the least lift value. Conversely, when the t/T is 0.25 and $Y = 2.0\%$ of c , the curve shows the broadest span of the pressure coefficient distribution envelope, accompanied by the most significant pressure differential between the upper and lower surfaces.

At a t/T of 0.75, the pressure coefficient distribution curve range is the largest for $Y = 0\%$ of c , leading to the foil experiencing the greatest lift value. However, when Y is greater than or equal to 1.0% of c , the pressure on the lower surface at the trailing edge is inferior to that on the upper surface. Consequently, the total pressure on the trailing edge is directed from the upper surface toward the lower surface. This results in the total pressure component on the trailing edge opposing the direction of the heaving velocity, hindering the uplift of the foil and reducing the energy harvesting effect.

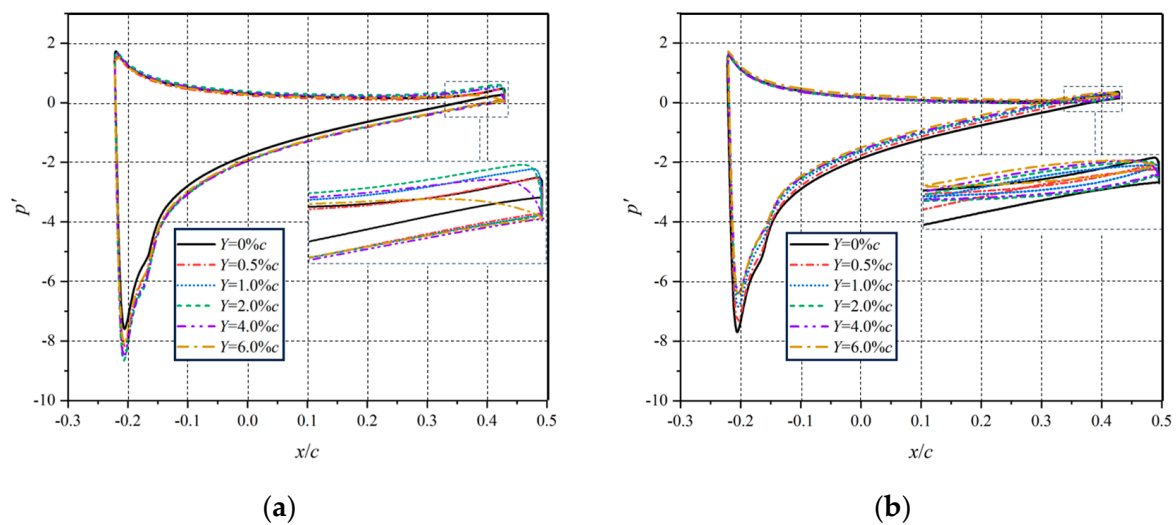


Figure 14. Distribution of the pressure coefficient on the surface of the oscillating foil with/without a cylindrical spoiler structure at the trailing edge for different cylinder longitudinal spacings. (a) $t/T = 0.25$; (b) $t/T = 0.75$.

3.4. Adaptability under Multiple Kinetic Parameters

Under the specified condition, the optimal configuration has been determined according to above analysis ($D = 11.0\%$ of c , $X = 0.5\%$ of c , $Y = 0$). The implementation of this configuration results in a notable enhancement in energy harvesting efficiency up to 19.26% compared to the case without the cylindrical spoiler structure. To further investigate whether the cylindrical spoiler structure is equally effective in terms of performance improvement for a wide range of flutter motion parameters, relatively conservative cylinder parameters ($D = 3.0\%$ of c , $X = 0.5\%$ of c , $Y = 0$) are chosen for this study instead of the optimal cylindrical spoiler structure parameters from the previous study. This approach allows for the further exploration of the adaptability of the trailing edge cylindrical structure under multiple kinetic parameters, and the purpose of not choosing the optimal trailing edge cylindrical structure is to minimize marginal effects and improve stability, while it can highlight the impact of different motion parameters on the energy harvesting performance.

To begin with, the aerodynamic performance of the oscillating foil with a trailing edge cylindrical spoiler structure ($D = 3.0\%$ of c , $X = 0.5\%$ of c , and $Y = 0$) is computed across a range of nondimensional reduced frequencies (f^*), from 0.2 to 1.0. Other parameters are kept constant to investigate the effectiveness of the new flow control method at various reduced frequencies. In Figure 15, the fluctuation of the energy harvesting efficiency is depicted as it varies with the nondimensional reduced frequency, both with and without the cylindrical spoiler structure.

The energy harvesting efficiency of the oscillating foil increases with the reduced frequency up to a certain point before decreasing. Specifically, the optimal efficiency of the foil with the cylindrical structure is found to be 8.17% higher than the one without, under the same operating parameters. This optimal energy harvesting efficiency for both types of foils is achieved at a reduced frequency of 0.6. Notably, at a reduced frequency of 0.2, the cylindrical turbulence structure provides the greatest relative increase of 22.39% in efficiency, as the oscillating foils are in a relatively low-level energy harvesting performance state.

It is worth mentioning that the energy harvesting efficiency of the oscillating foil equipped with the trailing edge cylindrical spoiler structure consistently surpasses that of the foil without for all the reduced frequencies examined in Figure 15. This suggests that the newly proposed flow control method, involving the use of cylindrical turbulence structures at the trailing edge of the oscillating foil, is effective over a broad range of reduced frequencies.

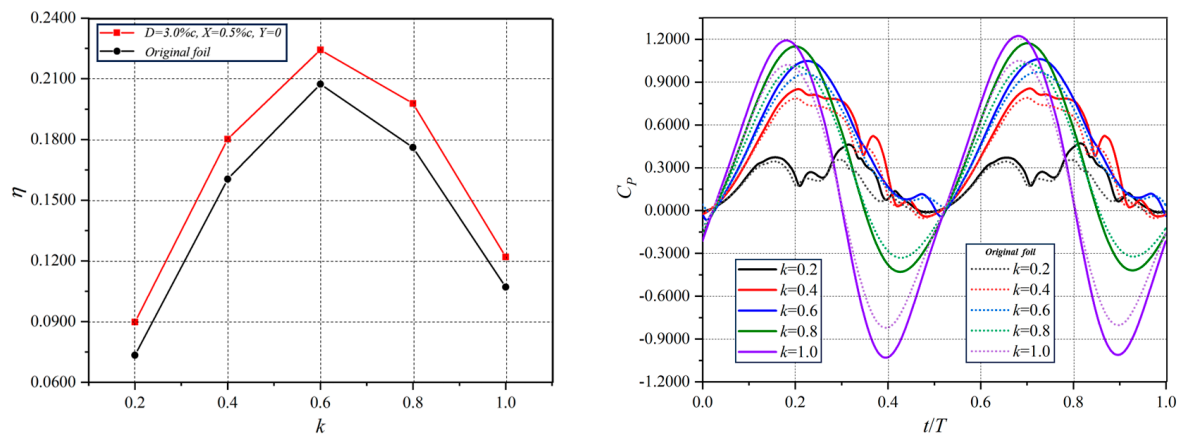


Figure 15. Energy harvesting efficiency of the oscillating foil with/without a cylindrical spoiler structure at the trailing edge for different reduced frequencies.

Subsequently, the aerodynamic performance of the oscillating foil with a trailing edge cylindrical spoiler structure ($D = 3.0\%$ of c , $X = 0.5\%$ of c , $Y = 0$) is computed across a wide range of relative heaving amplitudes (H/c), spanning from 0.2 to 1.4, as illustrated in Figure 16. The depicted trend in the figure reveals that the efficiency of the oscillating foil initially increases, followed by a subsequent decrease, with the rise in the relative heaving amplitude.

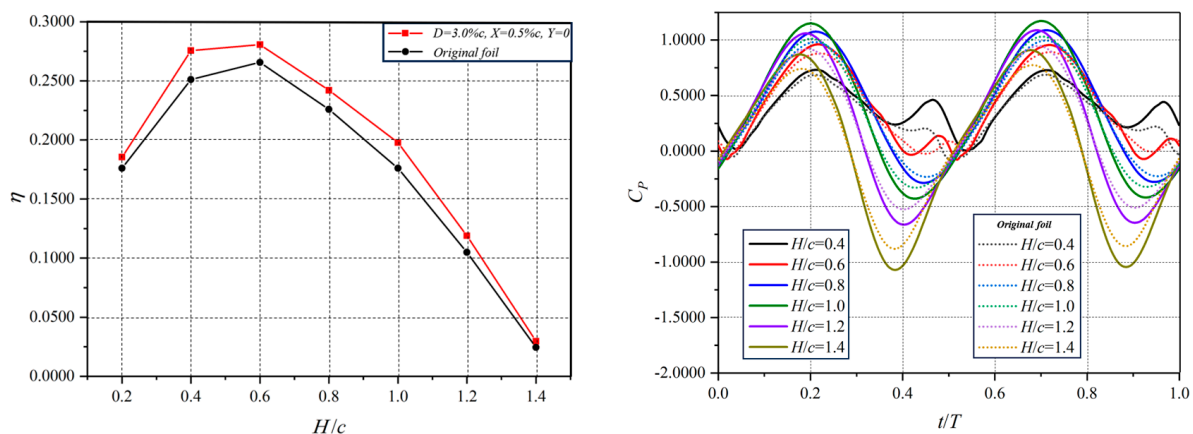


Figure 16. Energy harvesting efficiency of the oscillating foil with/without a cylindrical spoiler structure at the trailing edge for different relative heaving amplitudes.

Furthermore, it is observed that the performance of the oscillating foil equipped with a cylinder at the trailing edge consistently outperforms that of the one without, across all the relative heaving amplitudes. Notably, at a relative heaving amplitude of 0.4, the efficiency difference between the oscillating foil with and without the cylindrical spoiler structure is at its maximum. At a relative heaving amplitude of 0.6, both tail configurations, with and without a cylinder, exhibit the best energy harvesting efficiency. Specifically, the optimal efficiency of the foil with the cylindrical spoiler structure is 5.68% higher than the one without under the same working conditions. Additionally, the maximum enhancement in energy harvesting efficiency occurs when the relative heaving amplitude is 1.4, reaching up to 21.60%.

Consequently, the new flow control method, involving the use of a trailing edge cylindrical spoiler structure, is demonstrated to be effective for enhancing the oscillating foil performance across different relative heaving amplitudes.

In Figure 17, the effects of pitching amplitudes (θ_0) on the energy harvesting performance for the oscillating foil with and without a cylindrical spoiler structure at the trailing

edge are illustrated. The pitching amplitude ranges from 50° to 90° , while maintaining the structural parameters of the turbulence cylinder at the trailing edge unchanged, and all the other parameters consistent with the previously outlined calculations.

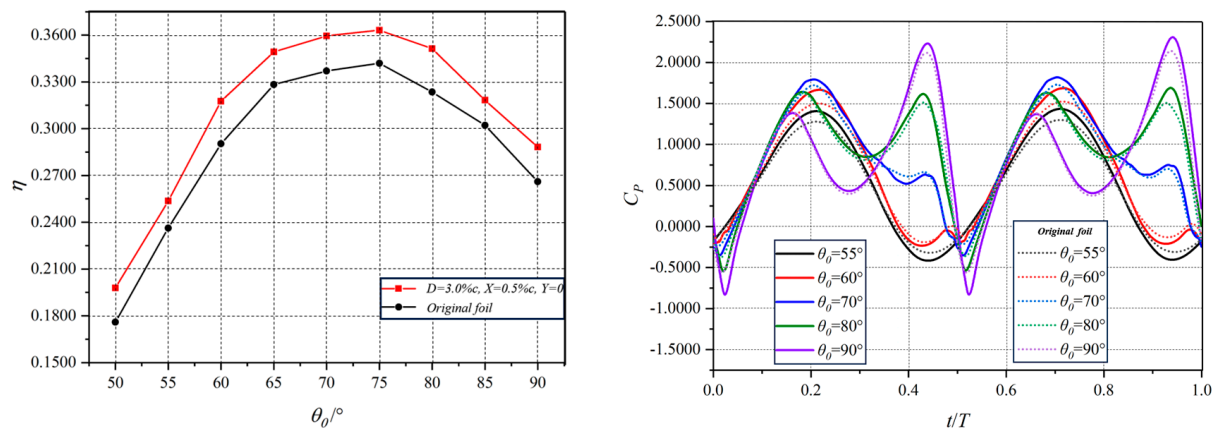


Figure 17. Energy harvesting efficiency of the oscillating foil with/without a cylindrical spoiler structure at the trailing edge for different pitching amplitudes.

Under the specified pitching amplitude conditions, the efficiency of the oscillating foil with a trailing edge cylindrical spoiler structure surpasses that of the one without. The energy harvesting efficiency demonstrates an initial increase, followed by a subsequent decrease with an augmentation in the pitching amplitude. Both types of oscillating foils reach their maximum efficiency at a pitching amplitude of 75° , with the oscillating foil equipped with the cylindrical spoiler structure exhibiting an optimal efficiency 6.20% higher than that without under the same conditions. The most substantial improvement occurs at a pitching amplitude of 50° , with an increase of 12.39%.

In summary, within the operating range of pitching amplitudes from 50° to 90° , the trends in energy harvesting efficiency for cylindrical and non-cylindrical oscillating foils remain consistent. Consequently, the new flow control method of enhancing energy harvesting performance through a cylindrical spoiler structure at the trailing edge is affirmed to be effective across various pitching amplitudes.

The aforementioned study conducts a comparative analysis of the aerodynamic performance of the oscillating foil with and without a designated cylindrical spoiler structure at the trailing edge across different motion parameters. The outcomes affirm the efficacy of the newly proposed flow control method, employing the cylindrical spoiler structure, in augmenting the performance of the oscillating foil for varying reduced frequencies, relative heaving amplitudes, and pitching amplitudes. The integration of the cylindrical spoiler structure at the trailing edge successfully enhances the energy harvesting capability of the system, underscoring the versatility and applicability of this novel flow control method for improving the energy harvesting efficiency of oscillating foils.

4. Conclusions

This study has successfully introduced a compact, efficient, and robust flow energy harvester, employing a novel flow control method featuring a cylindrical spoiler structure positioned at the trailing edge of the oscillating foil:

1. A notable enhancement of 19.26% has been achieved in the efficiency of the oscillating foil with the cylindrical spoiler structure at the trailing edge, utilizing a cylinder diameter of 11.0% of c , a transverse spacing of 0.5% of c , and a longitudinal spacing of 0.
2. It is crucial to highlight that an increase in cylinder diameter corresponds to an augmentation in energy harvesting efficiency, although with diminishing returns.
3. The variation in transverse spacing demonstrates a non-linear relationship with the energy harvesting efficiency of the oscillating foil. Within the examined range of 3.5%

to 65.5% of the chord length, the cylindrical spoiler structure has shown no positive impact on the energy harvesting performance. Practical applications should carefully consider transverse spacing based on specific requirements.

4. Increasing the longitudinal spacing of the cylinder results in the trailing edge cylinder deviating from the mid-chord, enhancing the energy harvesting performance during the first half-cycle while causing a corresponding decrease in the second half-cycle. However, the overall integrated energy harvesting performance remains superior to that of the original foil without the cylinder. It is important to note that the degree of improvement diminishes as the longitudinal spacing of the cylinders increases.
5. The innovative flow control technique, incorporating a cylindrical spoiler structure at the trailing edge of the oscillating foil, has proven highly effective in enhancing energy harvesting performance across various reduced frequencies, relative heaving amplitudes, and pitching amplitudes.

The findings of this study provide valuable insights for the design, optimization, and adaptability assessment of oscillating foil energy harvesting devices. We posit that this flow control method opens new avenues for the development of more efficient and practical oscillating foil devices. Future research endeavors could focus on conducting additional experimental measurements to evaluate and address uncertainties associated with numerical simulation calculations.

Author Contributions: Conceptualization, F.Z. and D.Z.; methodology, F.Z.; software, H.L.; validation, F.Z., H.L. and Q.Z.; formal analysis, F.Z.; investigation, H.L.; resources, Q.Z.; data curation, F.Z. and H.L.; writing—original draft preparation, F.Z. and Q.Z.; writing—review and editing, F.Z. and D.Z.; visualization, Q.Z.; supervision, Y.X. and D.Z.; project administration, D.Z.; funding acquisition, Y.X. All authors have read and agreed to the published version of the manuscript.

Funding: This research was funded by National Natural Science Foundation of China (grant number: 11872294).

Data Availability Statement: Data are contained within the article.

Conflicts of Interest: The authors declare no conflict of interest.

References

1. Moriarty, P.; Honnery, D. Can Renewable Energy Power the Future? *Energy Policy* **2016**, *93*, 3–7. [\[CrossRef\]](#)
2. Ellabban, O.; Abu-Rub, H.; Blaabjerg, F. Renewable Energy Resources: Current Status, Future Prospects and Their Enabling Technology. *Renew. Sustain. Energy Rev.* **2014**, *39*, 748–764. [\[CrossRef\]](#)
3. Abdelkefi, A. Aeroelastic Energy Harvesting: A Review. *Int. J. Eng. Sci.* **2016**, *100*, 112–135. [\[CrossRef\]](#)
4. McKinney, W.; DeLaurier, J. Wingmill: An Oscillating-Wing Windmill. *J. Energy* **1981**, *5*, 109–115. [\[CrossRef\]](#)
5. Young, J.; Lai, J.C.S.; Platzer, M.F. A Review of Progress and Challenges in Flapping Foil Power Generation. *Prog. Aerosp. Sci.* **2014**, *67*, 2–28. [\[CrossRef\]](#)
6. Peng, Z.; Zhu, Q. Energy Harvesting through Flow-Induced Oscillations of a Foil. *Phys. Fluids* **2009**, *21*, 123602. [\[CrossRef\]](#)
7. Jones, K.; Platzer, M.; Jones, K.; Platzer, M. Numerical Computation of Flapping-Wing Propulsion and Power Extraction. In Proceedings of the 35th Aerospace Sciences Meeting and Exhibit, Reno, NV, USA, 6–9 January 1997; American Institute of Aeronautics and Astronautics: Reno, NV, USA, 1997.
8. Davids, S.T. A Computational and Experimental Investigation of a Flutter Generator. Ph.D. Thesis, Naval Postgraduate School, Monterey, CA, USA, 1999.
9. Tuncer, I.H.; Kaya, M. Optimization of Flapping Airfoils For Maximum Thrust and Propulsive Efficiency. *AIAA J.* **2005**, *43*, 2329–2336. [\[CrossRef\]](#)
10. Dumas, G.; Kinsey, T. Eulerian Simulations of Oscillating Airfoils in Power Extraction Regime. In *Advances in Fluid Mechanics VI*; WIT Press: Skiathos, Greece, 2006; Volume 52, pp. 245–254.
11. Kinsey, T.; Dumas, G. Parametric Study of an Oscillating Airfoil in Power Extraction Regime. *AIAA J.* **2008**, *46*, 1318–1330. [\[CrossRef\]](#)
12. Simpson, B.J.; Hover, F.S.; Triantafyllou, M.S. Experiments in Direct Energy Extraction through Flapping Foils. In Proceedings of the Eighteenth International Offshore and Polar Engineering Conference, Vancouver, BC, Canada, 6–11 July 2008.
13. Zhu, Q. Optimal Frequency for Flow Energy Harvesting of a Flapping Foil. *J. Fluid Mech.* **2011**, *675*, 495–517. [\[CrossRef\]](#)
14. Wang, H.; Zheng, X.; Pröbsting, S.; Hu, C.; Wang, Q.; Li, Y. An Unsteady RANS Simulation of the Performance of an Oscillating Hydrofoil at a High Reynolds Number. *Ocean Eng.* **2023**, *274*, 114097. [\[CrossRef\]](#)

15. Li, K.; Zhou, D.; Sun, X. Performance Characteristics of Flapping Foil Flow Energy Harvester That Mimics Movement of Swimming Fish. *Ocean Eng.* **2023**, *280*, 114850. [\[CrossRef\]](#)
16. Yang, W.; Song, B.; Song, W.; Wang, L. The Effects of Span-Wise and Chord-Wise Flexibility on the Aerodynamic Performance of Micro Flapping-Wing. *Chin. Sci. Bull.* **2012**, *57*, 2887–2897. [\[CrossRef\]](#)
17. Le, T.; Ko, J.; Byun, D. Morphological Effect of a Scallop Shell on a Flapping-Type Tidal Stream Generator. *Bioinspir. Biomim.* **2013**, *8*, 036009. [\[CrossRef\]](#) [\[PubMed\]](#)
18. Le, T.Q.; Ko, J.H. Effect of Hydrofoil Flexibility on the Power Extraction of a Flapping Tidal Generator via Two- and Three-Dimensional Flow Simulations. *Renew. Energy* **2015**, *80*, 275–285. [\[CrossRef\]](#)
19. Hoke, C.M.; Young, J.; Lai, J.C.S. Effects of Time-Varying Camber Deformation on Flapping Foil Propulsion and Power Extraction. *J. Fluids Struct.* **2015**, *56*, 152–176. [\[CrossRef\]](#)
20. Liu, W.; Xiao, Q.; Zhu, Q. Passive Flexibility Effect on Oscillating Foil Energy Harvester. *AIAA J.* **2016**, *54*, 1172–1187. [\[CrossRef\]](#)
21. Jeanmonod, G.; Olivier, M. Effects of Chordwise Flexibility on 2D Flapping Foils Used as an Energy Extraction Device. *J. Fluids Struct.* **2017**, *70*, 327–345. [\[CrossRef\]](#)
22. Bai, X.-D.; Zhang, J.-S.; Zheng, J.-H.; Wang, Y. Energy Extraction Performance of a Flapping Wing with Active Elastic Airbag Deformation at the Leading Edge. *Ocean Eng.* **2021**, *228*, 108901. [\[CrossRef\]](#)
23. Jiang, W.; Wang, Y.L.; Zhang, D.; Xie, Y.H. Numerical Investigation into Power Extraction by a Fully Passive Oscillating Foil with Double Generators. *Renew. Energy* **2019**, *133*, 32–43. [\[CrossRef\]](#)
24. Liebeck, R.H. Design of Subsonic Airfoils for High Lift. *J. Aircr.* **1978**, *15*, 547–561. [\[CrossRef\]](#)
25. Lee, Y.-T.; Ahuja, V.; Hosangadi, A.; Ebert, M. Shape Optimization of a Multi-Element Foil Using an Evolutionary Algorithm. *J. Fluids Eng.* **2010**, *132*, 051401. [\[CrossRef\]](#)
26. Xiao, Q.; Liu, W.; Incecik, A. Flow Control for VATT by Fixed and Oscillating Flap. *Renew. Energy* **2013**, *51*, 141–152. [\[CrossRef\]](#)
27. Wu, J.; Zhan, J.P.; Wang, X.; Zhao, N. Power Extraction Efficiency Improvement of a Fully-Activated Flapping Foil: With the Help of an Auxiliary Rotating Foil. *J. Fluids Struct.* **2015**, *57*, 219–228. [\[CrossRef\]](#)
28. Xie, Y.H.; Jiang, W.; Lu, K.; Zhang, D. Numerical Investigation into Energy Extraction of Flapping Airfoil with Gurney Flaps. *Energy* **2016**, *109*, 694–702. [\[CrossRef\]](#)
29. Zhu, B.; Huang, Y.; Zhang, Y. Energy Harvesting Properties of a Flapping Wing with an Adaptive Gurney Flap. *Energy* **2018**, *152*, 119–128. [\[CrossRef\]](#)
30. Lahooti, M.; Kim, D. Multi-Body Interaction Effect on the Energy Harvesting Performance of a Flapping Hydrofoil. *Renew. Energy* **2019**, *130*, 460–473. [\[CrossRef\]](#)
31. Sun, G.; Wang, Y.; Xie, Y.; Lv, K.; Sheng, R. Research on the Effect of a Movable Gurney Flap on Energy Extraction of Oscillating Hydrofoil. *Energy* **2021**, *225*, 120206. [\[CrossRef\]](#)
32. Deng, J.; Teng, L.; Pan, D.; Shao, X. Inertial Effects of the Semi-Passive Flapping Foil on Its Energy Extraction Efficiency. *Phys. Fluids* **2015**, *27*, 053103. [\[CrossRef\]](#)
33. Ye, X.; Hu, J.; Zheng, N.; Li, C. Numerical Study on Aerodynamic Performance and Noise of Wind Turbine Airfoils with Serrated Gurney Flap. *Energy* **2023**, *262*, 125574. [\[CrossRef\]](#)
34. Sagmo, K.F.; Storli, P.-T.S. An Experimental Study Regarding the Effect of Streamwise Vorticity on Trailing Edge Vortex Induced Vibrations of a Hydrofoil. *J. Sound Vib.* **2023**, *542*, 117349. [\[CrossRef\]](#)
35. Jiang, W.; Yue, Y.; Xie, D.; Hou, Y. Fully-Passive Tethered Flapping Airfoil to Harvest High-Altitude Wind Energy. *Energy Convers. Manag.* **2022**, *267*, 115940. [\[CrossRef\]](#)
36. Wu, X.; Zhang, X.; Tian, X.; Li, X.; Lu, W. A Review on Fluid Dynamics of Flapping Foils. *Ocean Eng.* **2020**, *195*, 106712. [\[CrossRef\]](#)
37. Kinsey, T.; Dumas, G. Computational Fluid Dynamics Analysis of a Hydrokinetic Turbine Based on Oscillating Hydrofoils. *J. Fluids Eng.* **2012**, *134*, 021104. [\[CrossRef\]](#)

Disclaimer/Publisher’s Note: The statements, opinions and data contained in all publications are solely those of the individual author(s) and contributor(s) and not of MDPI and/or the editor(s). MDPI and/or the editor(s) disclaim responsibility for any injury to people or property resulting from any ideas, methods, instructions or products referred to in the content.